Spectral and polarization structure of field-induced photonic bands in cholesteric liquid crystals

S. P. Palto,* M. I. Barnik, A. R. Geivandov, I. V. Kasyanova, and V. S. Palto
Shubnikov Institute of Crystallography, RAS, Leninsky prospekt 59, 119333 Moscow, Russia
(Received 8 May 2015; revised manuscript received 2 July 2015; published 14 September 2015)

Transmission of planar layers of cholesteric liquid crystals is studied in pulsed electric fields perpendicular to the helix axis at normal incidence of both linearly polarized and unpolarized light. Spectral and light polarization properties of the primary photonic band and the field-induced bands up to fourth order of Bragg selective reflection are studied in detail. In our experiments we have achieved an electric field strength several times higher than the theoretical values corresponding to the critical field of full helix unwinding. However, the experiments show that despite the high strength of the electric field applied the helix does not unwind, but strongly deforms, keeping its initial spatial period. Strong helix deformation results in distinct spectral band splitting, as well as very high field-induced selective reflectance that can be applied in lasers and other optoelectronic devices. Peculiarities of inducing and splitting the bands are discussed in terms of the scattering coefficient approach. All observed effects are confirmed by numerical simulations. The simulations also show that liquid crystal surface anchoring is not the factor that prevents the helix unwinding. Thus, the currently acknowledged concept of continuous helix unwinding in the electric field should be reconsidered.

DOI: 10.1103/PhysRevE.92.032502 PACS number(s): 42.70.Df, 42.15.Eq, 42.79.Kr, 78.67.Pt

I. INTRODUCTION

A spontaneous helical distribution of the director field is a unique property of chiral liquid crystals (CLCs) [1,2]. It is well known that there is a forbidden spectral zone (stopband) for light propagating along the axis of the helix with pitch P in the spectral range $n_\parallel P \geqslant \lambda \geqslant n_\perp P$ ($n_\parallel$ and $n_\perp$ are the principal refractive indices respectively parallel and perpendicular to the liquid crystal director). In the spectral range of the stopband the propagation of circularly polarized light of the same handedness as that of the helix is forbidden [2,3], and it experiences Bragg reflection from the CLC layer. Light having the orthogonal circular polarization propagates through the layer with no reflection. It is also important that for light propagating along the helix axis there is the only a selective reflection band within the whole spectral range, which corresponds to the first Bragg order ($m = 1$). Below we refer to this band as the primary selective reflection band, and the corresponding spectral range as the primary photonic band. Higher-order reflection bands in the spectral ranges $(n_\parallel P)/m \geqslant \lambda \geqslant (n_\perp P)/m$, where m belongs to the set of natural numbers greater than 1, are forbidden [2,4]. However, under the condition that helical distribution of the LC director is distorted (e.g., under external magnetic or electric field perpendicular to the helix axis), the higher-order selective reflection bands become allowed.

Induction of high-order selective reflection bands was studied most thoroughly in theoretical works [5–8]. We consider works [7,8], which predict "triplet" structure of field-induced spectral bands, as most important. According to [7,8], three sub-bands in each band of order m are characterized by different light polarization properties: in the middle sub-band all the polarizations are reflected, while the two side sub-bands correspond to reflection of mutually orthogonal linearly polarized light. For a long time these theoretical predictions had not been confirmed experimentally. All that was reported in a number of publications [9–12] was related to observations of weak and not structured bands of the second order. However, recently the predictions of [7,8] have been confirmed experimentally [13], owing to an approach utilizing pulsed electric fields.

One should note that the above-mentioned theoretical studies were performed within the theoretical concept of the continuous helix unwinding in an electric field and the existence of the critical field E_c, above which the cholesteric helix is fully unwound. Therefore, for example, the primary selective reflection band was predicted to monotonically shift toward longer wavelengths due to field-induced increase of the helix pitch P [14–18]. Upon achieving the field E_c the full helix unwinding and disappearance of selective reflection were expected. Also it should be noticed that the theoretical concept of continuous unwinding [15] was developed for an infinite helix. However, it is known that in real systems, where the CLC layer is confined and there is LC surface interaction with substrates, the continuous unwinding of a helix can be forbidden [19–21]. For example, under temperature variations, when the natural pitch P_0 changes, the equilibrium pitch P in the layer can vary only in discrete steps–due to the energy barrier of the surface anchoring [19,20]. Moreover, at symmetrical boundary conditions the temperature-induced transitions are allowed only between the helix configurations distinguished by integer numbers of full helix turns [20]. However, in the case of temperature variations a bulk torque contribution caused by an elastic term associated with the natural twisting number (q_0) is changed monotonically, and the continuous helix unwinding is still available. For example, in [22] the possibility of suppressing the jumplike unwinding due to the change of twisting number q_0 is demonstrated at boundary conditions with strongly asymmetric anchoring strength. The pitch transitions at asymmetric boundary conditions with strong and weak anchoring are also studied under mechanical strain in the work [23] showing that at the weak anchoring surface the twist angle can be varied either discontinuously or by slipping depending on an LC layer thickness.

*serguei.palto@gmail.com

The case of the helix unwinding in an electric field has a principal difference from that caused by changing the q_0 number. The appearance of an electric field torque that can result in continuous unwinding anchoring is not evident even in the case of absence of surface anchoring, especially if one deals with a quadratic-in-field interaction. Nevertheless, there are publications where the continuous helix unwinding in an electric field is reported. For example, in the experimental study [24] both nonuniform and uniform helix unwinding are claimed depending on the gradients of the electric field applied. The authors studied LC cells of different thicknesses with different interdigitated electrode periodicity and came to the conclusion that the inhomogeneous unwinding is associated with strong gradients of the electric field. They also have found a good agreement between theoretical and experimental dependences of the helical pitch versus electric field magnitude. Although the authors of [24] consider the unwinding process at small field gradients as uniform, we are skeptical regarding this conclusion, because all the experimental spectra shown in the paper are characteristic for inhomogeneous (nonmonodomain) texture.

To our mind, although a CLC helix is metastable in an electric field (the unwound state has a minimum free energy at fields above E_c), due to the quadratic-in-field interaction there is no electric force (torque) that can shift (rotate) the molecules aligned along the field vector in order to change the initial (field-off) pitch of the helix. Thus, thermal fluctuations, defects in the CLC and at alignment surfaces, seem to be the only reasons pushing the helix to the thermodynamically stable unwound state. Our experimental and numerical results, which are shown below, strongly support this point of view.

This paper is organized as follows. First we describe the design of experimental cells, properties of liquid crystal materials, and the experimental technique for pulsed electric field driving. Then we discuss the experimental transmittance spectra measured for different light polarizations. In the last section we present the results of numerical simulations and explain experimental data in terms of scattering coefficient concept [4].

II. EXPERIMENTAL METHODS

The scheme of the experimental cell is shown in Fig. 1. The pulsed electric field E in the CLC layer is created by a pulse modulated sinusoidal voltage of a frequency of 24 kHz. The pulse duration $\tau = 2$ ms, and its repeating frequency $f = 10$ Hz. The voltage is applied to two planar aluminum electrodes (1) located at the inner surface of glass substrates

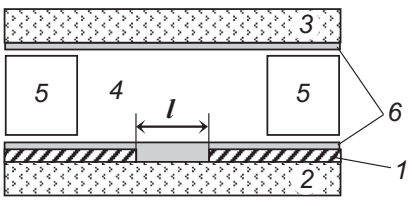

FIG. 1. Scheme of experimental LC cell: (1) aluminum electrodes; (2, 3) glass substrates; (4) CLC layer; (5) Teflon gaskets; (6) polyimide films.

(2). Vacuum deposited aluminum electrodes of a thickness of 100 nm are nontransparent in the visible and near-infrared spectral range. The distance between the electrodes ($l = 116\,\mu$m) is significantly larger compared to the CLC layer thickness ($d = 12\,\mu$m), which ensures sufficient homogeneity of the planar electric field. The thickness of the CLC layer (4) is defined by a gap between the two substrates, which is controlled by Teflon gaskets (5). The uniform orientation of CLC molecules in planes of the substrates, as well as the helix axis perpendicular to the substrates, is ensured by rubbed 50-nm thick polyimide films (6). The LC cell is assembled in such a way that the rubbing directions at the top and bottom surfaces are mutually opposite and parallel to the slit between the electrodes. Optical quality of the LC alignment is controlled by observations of the LC texture between two crossed polarizers.

The transmittance spectra are detected using an AvaSpec 2048 optic fiber spectrometer in the external trigger mode synchronously with the field pulses. Spectra measurement setup is based on a Polam 113 microscope (LOMO, Russia) with built-in incandescent lamp (20 W) as the light source. A ninefold magnification lens is used. Light propagated through the LC layer is focused with the microscope lens to the optical fiber of the spectrometer. A Glan prism is used to get linearly polarized incoming light. The glass optics of the microscope and the properties of the photosensitive matrix of the spectrometer limit measurements i to the spectral range from 400 to 1050 nm. Spectra are acquired during time intervals of the electric field pulses (2 ms) with a delay of 0.5 ms to the pulse front edge. This delay is required for getting equilibrium distribution of the LC director. We use home-made virtual instrument software that allows a multifunction arbitrary waveform generator and oscilloscope. A broadband amplifier based on a high-voltage operational amplifier (Apex PA85) is used to amplify the voltage up to 100 V. For further increase of the voltage amplitude up to 600 V a pulse transformer is applied.

Spectral studies are performed for two liquid crystal materials with helix pitch $P = 590$ and 1075 nm. CLC mixtures are produced by doping LC material E7 (Merck) with left-handed optically active compound α-bis(2-chloro-4-methylpentyl)biphenyl-4,4′-dicarboxylate in the amount of 14.1 and 7.2 wt % respectively. The resulted mixtures exhibit phase transition from chiral nematic to isotropic phase at 44 °C and 50 °C for 590 and 1075 nm pitch, respectively. Principal refractive indices of CLC at wavelength $\lambda = 589$ nm are: $n_\parallel = 1.713$ and $n_\perp = 1.530$ ($P = 590$ nm); $n_\parallel = 1.726$ and $n_\perp = 1.532$ ($P = 1075$ nm). Refractive indices are measured with an Abbé refractometer (Atago 1T, Japan) at temperature $T = 24$ °C. Spectral measurements are performed at $T = 24$ °C as well. In order to clarify some features of selective reflection the spectral measurements are also done for E7 mixtures with the right-handed optically active compound 1,4:3,6-dianhydro-D-sorbitol-2,5-bis(4-hexyloxybenzoate).

Transmittance spectra are measured relative to the air, i.e. the baseline is recorded without the sample. Since the beam aperture is slightly greater than the gap l between fully nontransparent (reflective) electrodes, partial reflection from the electrodes leads to the measured transmittance (relative to the air) in the spectral region of total transparency of the

CLC layer of about 70% instead of 91% (the value 91% follows from the sum of reflection coming from four interfaces: air-glass, glass-CLC, CLC-glass, and glass-air; which is about 9%). Because of the latter, all spectral curves presented in this work are normalized to the transmittance value of 91% at a wavelength of 700 nm (at this wavelength there is no selective reflection from the CLC layer, and its transmittance is limited only by reflection from the glass-substrate boundaries). This normalization facilitates comparison of curves and gives an indication of the absolute values of the selective reflectance of the CLC layers.

III. EXPERIMENTAL RESULTS

A. Unpolarized light

Transmittance spectra of a CLC layer with helix pitch $P = 590\,\text{nm}$ are presented in Fig. 2(a). In the absence of electric field ($U = 0\,\text{V}$) there is the primary photonic band with a transmittance of 50% in a range of 900−1000 nm. This transmittance relates to total selective reflectance of left-handed circularly polarized light. The photonic band is centered at $\lambda = 955\,\text{nm}$. When an electric field $E \cong 1.7\,\text{V}/\mu\text{m}$ is applied, very small additional transmittance reduction takes place in the middle of the primary photonic band (curve 2). This transmittance reduction significantly increases with further field growth (curve 4). Thus, the spectral splitting of the primary selective reflection band occurs. It should be noted that the field producing the pronounced splitting is above the critical field [4]:

$$E_c = \frac{\pi^2}{P}\sqrt{\frac{K_2}{\varepsilon_0(\varepsilon_\parallel - \varepsilon_\perp)}}, \tag{1}$$

where K_2 is the twist elastic coefficient, $\varepsilon_0 \cong 8.85 \times 10^{-12}\,\text{F/m}$ (in this work we use the SI system of units). Given the following parameters for the E7 LC material: $\varepsilon_\parallel - \varepsilon_\perp \cong 14.4$, $K_2 \cong 5.5\,\text{pN}$ [25], and $P \cong 590\,\text{nm}$, according to Eq. (1) one can estimate the critical field value as $E_c \cong 3.5\,\text{V}/\mu\text{m}$.

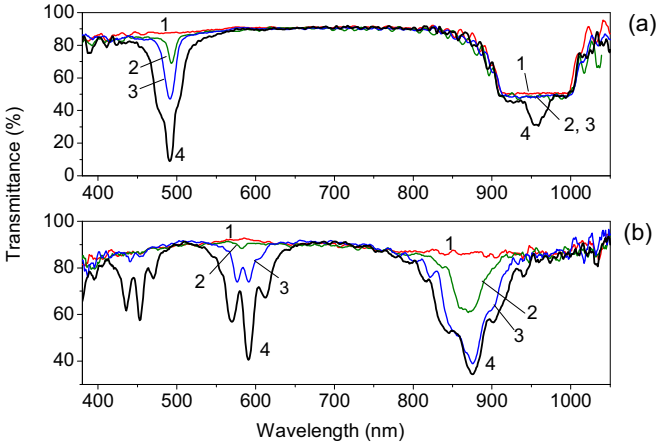

FIG. 2. (Color online) Transmittance spectra of CLC (a) with helix pitch 590 nm (primary and second-order photonic bands) and (b) with helix pitch 1075 nm (photonic bands of second, third, and fourth order) in unpolarized light at different electric field strengths: 1, $0\,\text{V}/\mu\text{m}$; 2, $1.7\,\text{V}/\mu\text{m}$; 3, $2.6\,\text{V}/\mu\text{m}$; 4, $5.2\,\text{V}/\mu\text{m}$.

At field $E = 5.2\,\text{V}/\mu\text{m}$, which is considerably higher than E_c, the transmittance is as low as 30%, i.e., about 70% of light is reflected. It is of utmost importance that the spectral position of the primary photonic band is not changed even at that high field. Thus no helix unwinding takes place.

Let us consider the effects in the spectral range of the field-induced second-order photonic band. We estimate a threshold electric field, at which a barely visible second-order-induced photonic band appears, at a level of $1.5\,\text{V}/\mu\text{m}$. At field $E = 2.6\,\text{V}/\mu\text{m}$ a narrow band with a minimum transmittance at $\lambda = 491\,\text{nm}$ is very pronounced, Fig. 2(a). Taking into account spectral dispersion of the refractive indices, this band corresponds to the second-order Bragg reflection. At fields above the critical field ($3.5\,\text{V}/\mu\text{m}$) the spectral band of the induced reflection is broadened, and spectral splitting into three sub-bands appears. This splitting is in good agreement with theoretical works [7,8], which predict triplet structure of the induced selective reflection bands. The minimum transmittance in the central sub-band decreases, achieving a value of 10% at $E = 5.2\,\text{V}/\mu\text{m}$. Since there are no signs of light scattering with increasing field (absence of scattering is confirmed by the transmittance remaining unchanged in a transparency region of 650−750 nm), we conclude that the field-induced reflection at a wavelength of 491 nm is up to 86% which is important for practical applications of this effect.

Unpolarized transmittance spectra of the CLC layer with pitch $P = 1075\,\text{nm}$ (with field-induced bands of the second, third, and fourth order being in a spectral range of 400−1000 nm) are given in Fig. 2(b). It is important to note that the double increase of the helix pitch leads, according to (1), to the double decrease of the critical field. We estimate the critical field for the given sample as $E_c \cong 1.8\,\text{V}/\mu\text{m}$. Thus, a field of $5.2\,\text{V}/\mu\text{m}$ achieved in the experiments corresponds to almost triple the critical field. Unfortunately, the primary selective reflection band at the given helix pitch is out of the recorded spectral region, and we are restricted to an analysis of the induced bands.

It follows from the given spectra that if the field is relatively low then the field-induced reflectance bands are represented by single bands. However, as the field increases all the induced bands show the pronounced triplet structure. The higher the order the more evident the splitting. Even the second-order band in a range of 800–950 nm has well-resolved triplet structure. The cause of more pronounced triplet splitting in the case of increased pitch ($P = 1075\,\text{nm}$ vs 590 nm) is higher helix deformation at the same electric field.

B. Linearly polarized light (e ∥ E and e ⊥ E)

The transmittance spectra of the CLC layer with helix pitch $P = 590\,\text{nm}$ for linearly polarized light (the electric field vector **e** is parallel to the external electric field vector **E**) are given in Fig. 3(a). When $E = 0$, the selective reflectance within the primary photonic band is not constant, and increases at the long-wavelength edge of the band. The increase of the electric field leads to further increasing the reflectance at the long-wavelength edge, as well as to the reflectance decrease at the short-wavelength edge. At $E = 5.2\,\text{V}/\mu\text{m}$ the transmittance at the long-wavelength band edge is about 20%, i.e., taking into account 5% reflectance from the internal and

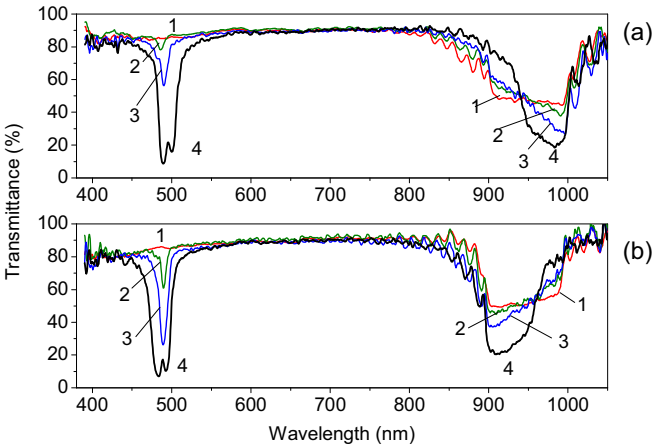

FIG. 3. (Color online) Transmittance spectra of CLC layer with a helix pitch of 590 nm (first- and second-order photonic bands) for (a) $\mathbf{e} \parallel \mathbf{E}$ and (b) $\mathbf{e} \perp \mathbf{E}$ at different electric field strengths: 1, 0 V/μm; 2, 1.7 V/μm; 3, 2.6 V/μm; 4, 5.2 V/μm.

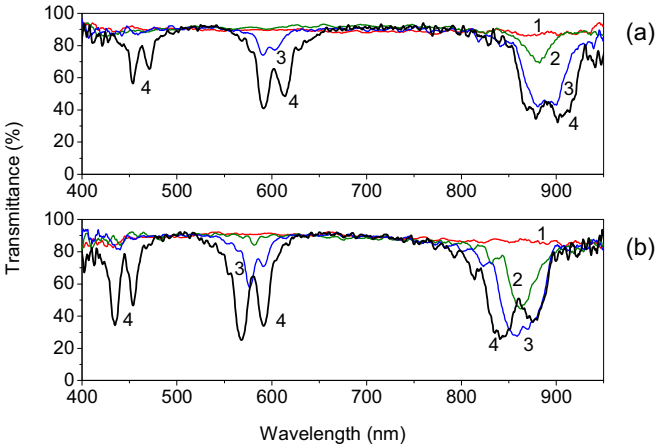

FIG. 4. (Color online) Transmittance spectra of CLC layer with helix pitch 1075 nm (photonic bands of the second, third, and fourth order) for (a) $\mathbf{e} \parallel \mathbf{E}$ and (b) $\mathbf{e} \perp \mathbf{E}$ at different electric field strengths: 1, 0 V/μm; 2, 1.7 V/μm; 3, 2.6 V/μm; 4, 5.2 V/μm.

external surfaces of the substrate, about 75% of the light is reflected by the CLC layer. Qualitatively, unless one considers the helix unwinding, such changes of the transmittance of the polarized light are in a good agreement with theoretical work [5], which studies the influence of the magnetic field on optical transmittance of CLCs. In contrast to the case of unpolarized light [Fig. 2(a)], where the reflection peak in the center of the primary band ($\lambda = 955$ nm) becomes well pronounced with increasing electric field, the central peak is barely seen because of higher reflectance at the long-wavelength band edge. For the orthogonal polarization ($\mathbf{e} \perp \mathbf{E}$) the spectral behavior at the edges of the photonic band is inverted, Fig. 3(b). Now, with the field increase the reflectance increases toward the short-wavelength band edge ($\lambda \sim 910$ nm).

One can observe the induction and splitting of the second-order reflection band in Fig. 3(a). Appearance of a narrow second-order reflection band with a minimum transmittance at $\lambda = 490$ nm (curves 2 and 3) is at a field of 1.7 V/μm. With further increasing the electric field the second-order band splits into two sub-bands. It is important to point out that the doublet component at wavelength $\lambda = 490$ nm corresponds to the central sub-band of the triplet in the case of the unpolarized light [Fig. 2(a)]. This component appears in both cases: $\mathbf{e} \parallel \mathbf{E}$, and $\mathbf{e} \perp \mathbf{E}$. If $\mathbf{e} \parallel \mathbf{E}$ then the second component of the doublet is shifted to the longer wavelengths [$\lambda = 500$ nm, Fig. 3(a)], otherwise ($\mathbf{e} \perp \mathbf{E}$) the shift is toward the shorter wavelengths [$\lambda = 480$ nm, Fig. 3(b)]. At high electric fields the reflectance in the second-order-induced bands is higher than that in the primary band. At $E = 5.2$ V/μm the reflectance in the central sub-band of the second order exceeds 90%.

For CLCs with helix pitch $P = 1075$ nm one can observe similar effects in the induced bands of the third and fourth order, Fig. 4. Owing to the higher degree of helix deformation, the field-induced band splitting is more pronounced. For both the orthogonal polarizations the central sub-bands of the second, third, and fourth orders are at 878, 590, and 453 nm respectively. Again, the spectral position of the second component of the doublet depends on the polarization: it is located at longer wavelengths, if $\mathbf{e} \parallel \mathbf{E}$, and at the shorter wavelengths for the orthogonal polarization ($\mathbf{e} \perp \mathbf{E}$). The spectral position of all the sub-bands coincides within an error of measurement with the spectral position of the sub-bands observed in unpolarized light.

C. Linearly polarized light (+45° and −45° angle between e and E).

Figure 5(a) shows the transmittance spectra of CLC layer with helix pitch $P = 590$ nm for the vector $\mathbf{e}$ at an angle $\varphi = +45$ with respect to the y axis. Our coordinate system is chosen so that the y axis is parallel to the cell substrate surfaces and is along the slit between the electrodes, the z axis is along the propagation of the light beam, and the x axis is along the electric field; clockwise rotation around z axis, when the observer looks along z, corresponds to positive sign of angle φ. When $E = 0$, the transmittance spectrum is similar to that for unpolarized light, Fig. 2(a). With increasing

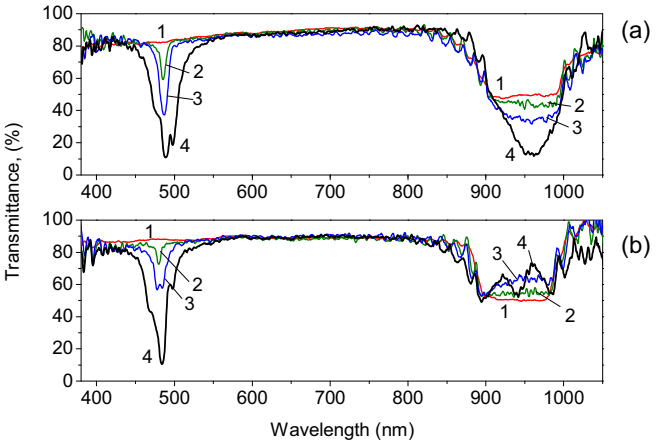

FIG. 5. (Color online) Transmittance spectra of CLC layer with helix pitch 590 nm (first- and second-order photonic bands) for (a) $\varphi = +45^\circ$ and (b) $\varphi = -45^\circ$ at different electric field strengths: 1, 0 V/μm; 2, 1.7 V/μm; 3, 2.6 V/μm; 4, 5.2 V/μm.

electric field the reflectance in the center of the primary band ($\lambda = 955$ nm) increases, and the band gradually becomes bell shaped. At low fields the second-order-induced photonic band ($\lambda = 485$ nm) is not split. At high fields (similarly to the case of unpolarized light) it splits into three sub-bands having transmittance minima at 480, 490, and 499 nm. The value of transmittance in the central sub-band at field $E = 5.2\,\mathrm{V}/\mu\mathrm{m}$ is reduced down to 12%. Thus, the reflectance is as high as 88% which is even higher than the reflectance in the center of the primary photonic band.

Transmittance spectra of CLC layers with helix pitch $P = 590$ nm in polarized light at $\varphi = -45$ are shown in Fig. 5(b). Here the reflectance in the primary photonic band decreases with increasing electric field, and this is the principal difference from the case $\varphi = +45$. At high electric fields the primary band exhibits a pronounced triplet structure with transmittance minima in the center and at the edges of the photonic band. We have observed experimentally that there is an inverse effect for right-handed CLCs: for $\varphi = -45$ the reflectance considerably increases as the field increases, and for $\varphi = +45$ the reflectance decreases and the primary band splits into the triplet.

IV. NUMERICAL SIMULATIONS AND ANALYSIS OF THE RESULTS

The experimental data presented above can be reproduced with high accuracy by numerical methods based on solution of the equations of LC continuum theory, as well as Maxwell's equations in the optical region. Our purpose is not only to explain the experimentally observed spectral dependences, but also to reveal the role of the surface anchoring in the observed stability of the helix pitch independently of the strength of the electric field.

For the simulations we use software based on the principles and algorithms described in [26,27]. The software is made by one of the authors (SPP) for solving a wide set of electro-optical problems in nematic and ferroelectric LCs [one- (1D) and three-dimensional LC designs on account of hydrodynamic backflow effects, flexoelectricity, arbitrary boundary conditions, and electric and dielectric properties of the alignment layers, complicate patterned electrode systems and others]. Optical calculations are based on the Berreman 4×4 matrix approach [28] with an algorithm described in [26]. It is worth mentioning that the software has been being intensively used in the Liquid Crystal Laboratory at IC RAS for more than 15 years, and it has been found to be quite reliable in predicting performance of real LC systems.

The purposes of the current work allow simplifications, so it is not necessary to discuss all the equations the software is based on. In our particular case we deal with 1D static problem (LC alignment is to be homogeneous in the xy plane, the hydrodynamic backflow coupling effects are neglected, so the solved set of equations is reduced to the following Euler-Lagrange equations in order to determine the static spatial distribution of the CLC director field $\mathbf{n}(z) = (n_x(z), n_y(z), n_z(z))$:

$$-\frac{\partial(F+g)}{\partial n_i} + \frac{d}{dz}\left(\frac{\partial(F+g)}{\partial n_i'}\right) = 0, \quad i \in \{x,y,z\}, \qquad (2)$$

where $n_i' = \partial n_i/\partial z$, $g = \frac{1}{2}\eta(1 - \sum_1 n_i^2)$, η is the Lagrange multiplier that is due to the unit length of the vector $\mathbf{n}$, and F is the free energy density in bulk of the LC, which in case of our geometry is reduced as

$$F = \frac{1}{2}K_2(\mathbf{n} \cdot \mathrm{rot}\,\mathbf{n} + q_0)^2 - \frac{(\varepsilon\mathbf{E}) \cdot \mathbf{E}}{2}. \qquad (3)$$

In Eq. (3) the first term describes the density of the elastic energy of the twist deformation of the CLC with wave number q_0 defining the natural helix pitch $P_0 = 2\pi/q_0$, and the second term is the contribution of the electric field energy on account of operation at a fixed voltage on the electrodes [in our case the field is along the x axis, $\mathbf{E} = (E_x, 0, 0)$]. The components of the dielectric permittivity tensor ε are related to the director components as follows:

$$\varepsilon_{ij}(z) = \varepsilon_\perp \delta_{ij} + (\varepsilon_{||} - \varepsilon_\perp) n_i(z) n_j(z), \qquad (4)$$

where δ_{ij} is the Kronecker delta.

Equations (2) are solved together with the equations at the layer boundaries:

$$-\frac{\partial F}{\partial \mathbf{n}'} \pm \frac{\partial W}{\partial \mathbf{n}} = 0, \qquad (5)$$

where W is the potential of the surface anchoring energy (the signs "+" and "−" correspond to opposite surfaces), which in the local coordinate system $x'y'z'$ related to the easy axis $\mathbf{R} \parallel y'$ at the surface of the substrate is

$$W = \tfrac{1}{2}W_a n_{x'}^2 + \tfrac{1}{2}W_z n_{z'}^2, \qquad (6)$$

where W_a and W_z are the amplitudes of the azimuthal and zenithal anchoring energy. The signs "+" and "−" in (5) are respectively for the first and the second surface of the CLC layers. Equation (6) corresponds to the well-known Rapini-Popoular (RP) model of the surface anchoring potential. In the used software the RP model is implemented for an arbitrary orientation of the local $x'y'z'$ frame defining the tilt angle of the easy axes as described in [27]. In our particular case the local coordinate system coincides with the laboratory one, since the y' axis is oriented along $\mathbf{R} \parallel y$, and the x' axis coincides with x.

The simulations for different values of the anchoring energy have not revealed its significant effect on the transmittance spectra. It should also be mentioned that even though the RP model is the simplest one, it remains adequate for our primary task to see what is happening when the anchoring strength is approaching a zero value. Unfortunately, we are not capable of making the simulations at exactly zero anchoring energy, because in this case the extrapolation anchoring length, which is involved into the set of equations, becomes infinite. Thus, we perform calculations for very high but finite values of the extrapolation anchoring length to ensure that the numerical solution remains stable.

We have found that in fields significantly higher than the critical field E_c, the helix pitch remains unchanged even at negligible anchoring energy. We consider this result as rather important. We believe that zeroing the anchoring energy and allowing free rotation of the director at the layer boundaries results in behavior when a confined helix is equivalent to an infinite helix, for which continuous unwinding is predicted [15] as the field approaches E_c. However, in our simulations,

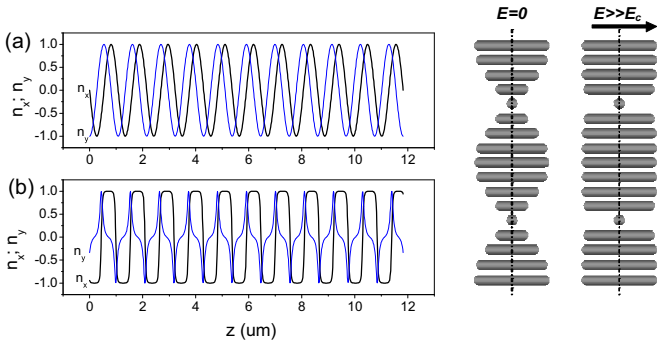

FIG. 6. (Color online) Simulated distribution of the director field in the CLC layer (the parameters correspond to the experimental sample with a pitch of 1.075 μm) (a) in the absence of the electric field and (b) at $E_x = 5.2\,\mathrm{V}/\mu\mathrm{m}$; simulation is performed for negligible LC surface anchoring ($W_a = W_z = 10^{-9}\,\mathrm{J/m^2}$). At the right side the schematic representation of the non-disturbed and field-distorted helix is shown.

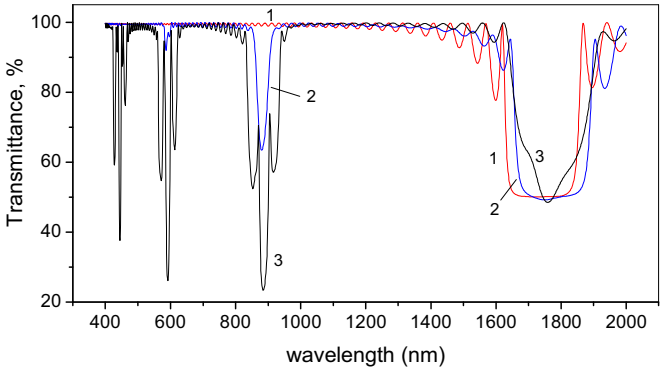

FIG. 7. (Color online) Transmittance spectra of the CLC layer in unpolarized light simulated for different electric field strengths. The CLC parameters correspond to the experimental sample [see Fig. 2(b)]. The CLC layer thickness equals 11 pitches with $P_0 = 1075\,\mathrm{nm}$ ($d = 11.875\,\mu$m). Curves: (1) $E_x = 0$; (2) $E_x = 1.7\,\mathrm{V}/\mu$m; (3) $E_x = 5.2\,\mathrm{V}/\mu$m. Simulations performed for negligible surface anchoring $W_a = W_z = 10^{-9}\,\mathrm{J/m^2}$.

as well as in the experiments, we do not observe any unwinding. Instead, a strong deformation of the helix occurs. It is confirmed with the calculations in Fig. 6 showing the CLC director distribution across the layer for extremely weak anchoring energy ($W = W_a = W_z = 10^{-9}\,\mathrm{J/m^2}$), when the typical extrapolation anchoring length ($K_2/W \cong 5500\,\mu$m) significantly exceeds not only the helix pitch, but also the LC layer thickness. In this case the director is not influenced by the boundaries, and its rotation at the surface is controlled solely by the elastic torque depending on elasticity modulus K_2 and wave number q_0 (this torque is controlled in the experiment by a chiral additive). As follows from the data in Fig. 6(a), in the absence of the electric field the director at the surfaces is along easy axes parallel to the y axis. We have adjusted the CLC layer thickness to be exactly equal to 11 pitches with $P_0 = 1.075\,\mu$m, in order to provide an equilibrium pitch P equal to P_0. Thus, in the absence of electric field, there is no surface torque regardless of the anchoring magnitude. At the electric field applied, if the anchoring is weak then the director is oriented almost along the electric field at the surfaces. However, even at extremely high electric fields [Fig. 6(b)] and negligible anchoring, despite the possibility of free "sliding" of the director at the surfaces, the director at the layer boundaries is not strictly along the field ($n_x < 1$ at $z = 0$ and $z = 11.825\,\mu$m). The latter is associated with the presence of torque due to the q_0 wave number causing the spontaneous formation of the helical structure. In the bulk of the layer, in planes where the director is strictly perpendicular to the field ($n_x = 0, n_y = 1$), the director is fixed regardless of the electric field strength. This leads to the fact that in very strong fields the n_x component distribution becomes close to the rectangular function, Fig. 6(b). The most important result is that there is no sign of helix unwinding even in the absence of the anchoring.

Optical transmittance spectra simulated for different values of the electric field strength are shown in Fig. 7. The parameters used for the simulations correspond to those of the experimental sample, except the anchoring is negligible. Therefore, the spectral curves in Fig. 7 can directly be compared to the experimental spectra [Fig. 2(b)], and they match very well.

The simulations reproduce in detail the appearance of high-order reflection bands in the electric field and its triplet splitting in accordance with the experiment. Nevertheless, we believe that for better understanding of the physical nature of the effect one could involve an approach based on scattering amplitude analysis [4]:

$$\alpha = \mathbf{f} \cdot \boldsymbol{\varepsilon}(\mathbf{q}) \cdot \mathbf{i}, \tag{7}$$

where $\mathbf{i}$ and $\mathbf{f}$ are the unit vectors describing polarization of the incident and scattered waves with corresponding wave vectors $\mathbf{k_0}$ and $\mathbf{k_1}$; $\mathbf{q} = \mathbf{k_0} - \mathbf{k_1}$ is the scattering wave vector, and $\boldsymbol{\varepsilon}(\mathbf{q})$ is the Fourier transform of the dielectric permittivity tensor.

According to the experiment, the CLC helix does not unwind, but deforms in the xy plane perpendicular to the helix axis. Therefore the spatial distribution of the LC director components $\mathbf{n}(z) = (n_x(z), n_y(z), 0)$ can be presented as a Fourier series:

$$n_x(z) = \sum_m A_m \cos[q_0(2m-1)z]; \quad n_y(z) = \left[1 - n_x^2(z)\right]^{1/2}, \tag{8}$$

where m is the set of natural numbers.

The director n_x component in Eq. (8) is presented by the sum of odd harmonics with amplitudes A_m depending on the field strength. However, as shown above, in intensive electric fields, significantly exceeding E_c, the distribution of $n_x(z)$ approaches a rectangular function. In this case the harmonic amplitudes are just those for the rectangular wave form:

$$A_m = \frac{4}{\pi(2m-1)}. \tag{9}$$

The spatial distribution of the components of the CLC director field explicitly determines the corresponding distribution of the dielectric permittivity tensor components (4), and the Fourier transform for the tensor components is

$$\varepsilon_{ij}(q) = \int_z \varepsilon_{ij}(z) \exp(iqz) dz. \tag{10}$$

In order to understand the appearance of the field-induced selective reflection bands, one can consider the simplest case of the series (8) restricted by the third harmonic, which is implemented in relatively weak fields (Fig. 7, curve 2). In this case, for example, $\varepsilon_{xx}(q)$ according to Eqs. (4) and (10) can be expressed as [21]

$$\begin{aligned}\varepsilon_{xx}(q) &= (\varepsilon_{||} - \varepsilon_{\perp}) \int_z [A_1 \cos(q_0 z) + A_3 \cos(3q_0 z)]^2 \exp(iqz) dz, \\ &= \varepsilon_a \left[\frac{A_1^2}{4} + \frac{A_1 A_3}{2} \right] \int_z \{\exp[(i(q+2q_0)z] + \exp[-i(q-2q_0)z]\} dz + \varepsilon_a \frac{A_1 A_3}{2} \int_z \{\exp[i(q+4q_0)z] \\ &\quad + \exp[-i(4q_0 - q)z]\} dz + \varepsilon_a \frac{A_3^2}{4} \int_z \{\exp[i(q+6q_0)z] + \exp[-i(6q_0 - q)z]\} dz. \end{aligned} \tag{11}$$

As follows from Eq. (11), the scattering coefficient is nonzero if $q = \pm 2q_0$, $q = \pm 4q_0$, and $q = \pm 6q_0$. Here the only case having physical meaning is $q = 2q_0$, $q = 4q_0$ and $q = 6q_0$. The case $q = 2q_0$ corresponds to first-order Bragg reflection when $k_0 = -k_1 = q_0$.

It can be easily seen from Eq. (11) that the integrals corresponding to the second and third order are nonzero only under the condition of the third harmonic of the director field distribution being nonzero. Thus, the presence of only first-order Bragg reflection in the case of the undisturbed helix follows from the harmonical (sinusoidal) distribution of the director components.

According to (11), the number of reflection orders is determined by the number of nonzero amplitudes in the Fourier expansion of the dielectric tensor, and herein we want to point out an interesting relation between the nonzero Fourier components of the dielectric tensor and the Fourier components of the distorted director field distribution, which is specific for the quadratic-in-field interaction in nematic CLCs. As follows from Eq. (11), the presence of the second-order Bragg reflection can be interpreted as a result of coupling between the first and third harmonics in the director field distribution [the second term in Eq. (11) is proportional to $A_1 A_3$]. Taking into account all the harmonics (9) one can realize that the appearance of even harmonics in optics [Eq. (11)] is due to coupling between odd harmonics in the LC director distribution. The induction of only odd harmonics in the distribution of the n_x component of the LC director is due to the purely quadratic type of interaction between the electric field and nematic CLCs. In the case of ferroelectric LCs the linear-in-field interaction results in both odd and even harmonics appearance in the Fourier spectrum of the n_x director distribution, and, in this sense, the nature of even optical harmonics would be different from that in nematic CLCs. It is also worth mentioning that in the case of the ferroelectrics our preliminary simulations show the possibility of continuous helix unwinding.

The fine spectral splitting within individual bands of mth-order Bragg reflection was explained in [7,8] in terms of the eigenmodes excited inside a distorted CLC. Herein we would like to involve a more simplified explanation of the fine splitting in terms of the photon optics [29]. To our mind, this approach provides another view on the physics and basic features of the splitting without complicated math.

Let a CLC be subjected to an extremely high electric field, so in the majority of the CLC volume the director is oriented along the electric field vector. In this case we can model a strongly deformed helix as a homogeneous anisotropic medium (matrix) with an inserted periodic stack of very thin anisotropic layers (walls) having the same principal refractive indices ($n_{||}$, $n_{\perp}$; note that the refractive indices are designated by the same symbols as the director components, but the nonitalic font is used) as the matrix, but the orientation of the local optical axes (the local optical axis coincides with $\varepsilon_{||}$—the principal axis of the local dielectric tensor) in these walls is continuously varied from that corresponding to the matrix to a perpendicular one, Fig. 8.

In terms of the normal (eigen) modes one can consider the four waves polarized along the x and y axes and propagating in forward and backward directions. In terms of the photon optics we are speaking of photons, which can be of arbitrary polarization—the photons that belong to the x-polarized mode

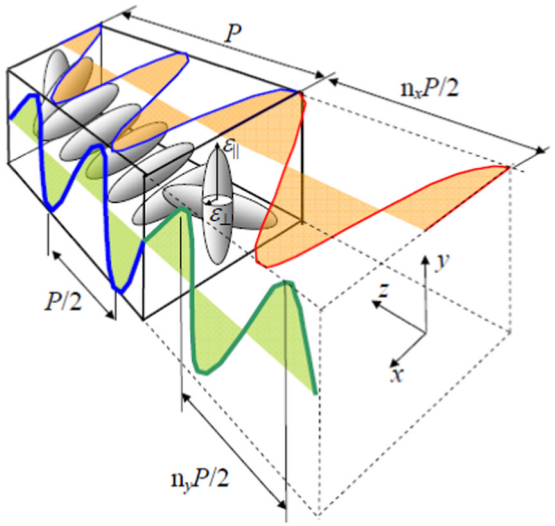

FIG. 8. (Color online) A scheme illustrating the spectral splitting of the field-induced second-order photonic band. One pitch of CLC helix deformed by an electric field applied along the x axis is shown inside the solid box. The dashed box confines free space. The standing waves which are due to the interference of forward and Bragg-reflected backward waves with wave vectors $k = \pm 4p/P$ inside the CLC medium are drawn at the box edges, and they have different wavelengths $n_x P/2$ and $n_y P/2$ respectively for x- and y-polarized light in the free space.

can be treated as superpositions of the photons polarized in two arbitrary orthogonal directions. Since we deal with plane waves propagating in the $+z$ and $-z$ directions, the momentum **k** of the photons is well defined at each z position for an arbitrary plane parallel to the xy plane (the xy position of the photons in these planes, of course, is undefined due to the indefiniteness principle). However, due to inhomogenity of the CLC medium in the z direction the magnitude of the momentum of the photons defining their phase velocity depends on z. For the last reason we speak of some effective value of the phase velocity averaged over z positions for a chosen polarization. We associate this average phase velocity with an effective value of the refractive index n_{eff}. The photons polarized along the x axis belong to the mode with waves propagating with c/n_x phase velocity (c is the speed of the light in free space, and n_x is an effective refractive index for the x-polarized photons; $n_x \cong n_\parallel$ when the optical anisotropy is small and the walls are extremely thin compared to the distance between them), whereas for the photons in the orthogonal mode the wave phase velocity is $c/n_y \cong c/n_\perp$. Thus the Bragg reflection frequencies of these photons and corresponding free space wavelengths are different, which results in different spectral position (spectral splitting) of these two modes, Fig. 8.

Unpolarized light can be treated as a sequence of independent photons with mutually orthogonal polarizations. To describe a response to the unpolarized light it is enough to consider two independent responses for two arbitrary but mutually orthogonal polarizations that result in zero values of the three components of the Stokes vector defining the light polarization state. In terms of the photon optics the choice of the two orthogonal directions can be arbitrary, but the probability of finding a photon polarized in a given direction is proportional to the intensity of the optical field in that direction. The statistical averaging of the velocity over independent photons under the assumption of equal number of photons in each of the orthogonal x and y modes gives a simple result $(1/n_x + 1/n_y)c/2 \cong (1/n_\parallel + 1/n_\perp)c/2$. Thus, one can define the effective refractive index for the unpolarized light as $n_{eff} \cong 2n_\parallel n_\perp/(n_\parallel + n_\perp)$. The averaging procedure performed is still approximate, because we have assumed equal probability to find a photon in each of the two orthogonal states inside of the anisotropic medium. As mentioned above, the probability to find the photon in a mode depends on the optical field intensity. While in the free space the optical field intensities and, as a result, the probabilities are equal indeed, in the case of an anisotropic medium the assumption is reasonable only if the optical anisotropy is sufficiently small: $(\delta n/n)^2 \ll 1$, where $n = (n_\parallel + n_\perp)/2$, $\delta n = (n_\parallel - n_\perp)/2$. On account of the last condition $n_{eff} = 2n_\parallel n_\perp/(n_\parallel + n_\perp) = n[1 - (\delta n/n)^2] \cong (n_\parallel + n_\perp)/2$. Thus, in the case of unpolarized light at strong CLC deformation one can separate three characteristic frequencies for mth-order Bragg reflected photons: (i) $mc/(Pn_\parallel)$, (ii) $mc/(Pn_\perp)$, and (iii) $2mc/[P(n_\parallel + n_\perp)]$. The photon frequency $2mc/[P(n_\parallel + n_\perp)]$ corresponds to the middle of the mth-order photonic band, and it also corresponds to the photons which are polarized in directions different from the x and y axes (on average at $\pm 45^\circ$ with respect to the x and y axes inside the layer). While the light scattering and Bragg reflection of the x- and y-polarized photons are ensured by the largest amplitude of the spatial modulation of the refractive index along the z axis, the reflected light intensity at the middle frequency is significant only if the orientation of the local optical axis is variable inside the walls. Only in this case can the momentum of a photon polarized, say, at 45° with respect to the x axis be changed by walls, and the Bragg reflection is possible. For example, if the walls are characterized by a dielectric tensor with principal axes exactly perpendicular to that of the matrix then the spatial distribution of the refractive index for the photons polarized at 45° is not modulated (constant), and they are not scattered by the walls. Thus, in this case instead of the three sub-bands only the two sub-bands at frequencies $mc/(Pn_\parallel)$ and $mc/(Pn_\perp)$ must be observed for the unpolarized light. Therefore, it is the variable distribution of the LC director inside the walls that is responsible for the spectral splitting into the triplet but doublet in the case of unpolarized light and the doublet splitting in the case of linearly polarized light.

V. CONCLUSION

To summarize, we have presented a detailed experimental study of the spectral and light polarization properties of field-induced selective reflection bands in chiral liquid crystals. By using pulsed electric driving and increasing the helix pitch, we have achieved an applied electric field that significantly exceeds the helix unwinding critical field without any sign of the helix unwinding. As a result, we have observed intense field-induced selective reflection bands up to fourth Bragg reflection order with very pronounced triple spectral splitting. We have experimentally confirmed the basic theoretical predictions for high-order band splitting and their polarization properties. We have also revealed additional features of the electric field influence on Bragg reflection in the primary photonic band. The experimental results have been confirmed by numerical simulations within continuum theory for liquid crystals and explained in terms of scattering coefficient approach. We would like to emphasize that according to our numerical simulations, even if the surface anchoring energy is negligible, there is still no helix unwinding at fields higher than the critical one. Thus, the transition from the in-field metastable state to the thermodynamically favorable unwound state is possible through defect formation only. In this regard, the classical concept of continuous helix unwinding that was made for an infinite helix should be reconsidered.

The described spectral-polarizing effects with controllable and high reflectance are characterized by submillisecond switching times. Thus, they are of practical interest for using in liquid crystal information display technology and in laser devices, where control of reflectance in a given spectral range is required.

ACKNOWLEDGMENT

The work has been supported by the Russian Science Foundation (Project No. 14-12-00553).

[1] P. G. de Gennes, *The Physics of Liquid Crystals* (Clarendon, Oxford, 1974).

[2] L. M. Blinov, *Structure and Properties of Liquid Crystals* (Springer, Berlin, 2011).

[3] V. A. Belyakov, *Diffraction Optics of Complex Structured Periodic Media* (Springer, Berlin, 1992).

[4] P. G. de Gennes and J. Prost, *The Physics of Liquid Crystals*, Oxford Science Publications (Clarendon, Oxford, 1993).

[5] S. C. Chou, L. Cheung, and R. B. Meyer, Effects of a magnetic field on the optical transmission in cholesteric liquid crystals, Solid State Commun. **11**, 977 (1972).

[6] R. Dreher, Reflection properties of distorted cholesteric liquid crystals, Solid State Commun. **12**, 519 (1973).

[7] S. Shtrikman and M. Tur, Optical properties of the distorted cholesteric structure, J. Opt. Soc. Am. **64**, 1178 (1974).

[8] V. A. Belyakov and V. E. Dmitrienko, Theory of the optical properties of cholesteric liquid crystals in an external field, Sov. Phys. Solid State **17**, 307 (1975).

[9] L. M. Blinov, S. V. Belyaev, and V. A. Kizel, High-order reflections from a cholesteric helix induced by an electric field, Phys. Lett. **65**, 33 (1978).

[10] S. V. Belyaev, L. M. Blinov, and V. A. Kizel, Observation of higher order Bragg reflection of light from a cholesteric liquid crystal induced by an electric field, JETP Lett. **29**, 310 (1979).

[11] M. Rumi, V. P. Tondiglia, L. V. Natarajan, T. J. White, and T. J. Bunning, Effects of in-plane electric fields on the optical properties of cholesteric liquid crystals, Proc. SPIE **8828**, 882817 (2013).

[12] M. Rumi, T. J. White, and T. J. Bunning, Reflection spectra of distorted cholesteric liquid crystal structures in cells with interdigitated electrodes, Opt. Express **22**, 16510 (2014).

[13] S. P. Palto, M. I. Barnik, A. R. Geivandov, and V. S. Palto, Induction of selective reflection bands by a pulsed electric field in layers of chiral liquid crystals, JETP Lett. **98**, 170 (2013).

[14] R. B. Meyer, Distortion of a cholesteric structure by a magnetic field, Appl. Phys. Lett. **14**, 208 (1969).

[15] P. G. de Gennes, Calcul de la distorsion d'une structure cholesterique par un champ magnetique, Solid State Comm. **6**, 163 (1968).

[16] A. M. Scarfone, I. Lelidis, and G. Barbero, Cholesteric-nematic transition induced by a magnetic field in the strong-anchoring model, Phys. Rev. E **84**, 021708 (2011).

[17] S. V. Belyaev and L. M. Blinov, Step unwinding of a spiral in a cholesteric liquid crystal, JETP Lett. **30**, 111 (1979).

[18] H. Xianyu, S. Faris, and G. P. Crawford, In-plane switching of cholesteric liquid crystals for visible and near-infrared applications, Appl. Opt. **43**, 5006 (2004).

[19] V. A. Belyakov and E. I. Kats, Surface anchoring and temperature variations of the pitch in thin cholesteric layers, JETP **91**, 488 (2000).

[20] S. P. Palto, On mechanisms of the helix pitch variation in a thin cholesteric layer confined between two surfaces, JETP **94**, 260 (2002).

[21] L. M. Blinov and S. P. Palto, Cholesteric Helix: Topological Problem, Photonics and Electro-optics, Liquid Cryst. **36**, 1037 (2009).

[22] A. D. Kiselev and T J. Sluckin, Twist of cholesteric liquid crystal cells: Stability of helical structures and anchoring energy effects, Phys. Rev. E **71**, 031704 (2005).

[23] I. Lelidis, G. Barbero, and A. L. Alexe-Ionescu, Cholesteric pitch transitions induced by mechanical strain, Phys. Rev. E **87**, 022503 (2013).

[24] M. Rumi, V. P. Tondiglia, L. V. Natarajan, T. J. White, and T. J. Bunning, Non-Uniform Helix Unwinding of Cholesteric Liquid Crystals in Cells with Interdigitated Electrodes, ChemPhysChem **15**, 1311 (2014).

[25] J. Parka, M. Dąbrowski, and R. Kowerdziej, Investigations of twist elastic constant K_{22} of new nematic liquid crystal materials using threshold IPS method, Opto-Electron. Rev. **19**, 114 (2011).

[26] S. P. Palto, An algorithm for solving the optical problem for stratified anisotropic media, JETP **92**, 552 (2001).

[27] S. P.Palto, Simulation of electrooptical effects and dynamics of ferroelectric liquid crystals, Crystallogr. Rep. **48**, 124 (2003).

[28] D. W. Berreman, Optics in stratified and anisotropic media: 4×4-matrix formulation, J. Opt. Soc. Am. **62**, 502 (1972).

[29] B. E. A. Saleh and M. C. Teich, *Fundamentals of Photonics* (John Wiley, New York, 1991).